Results in Optics 12 (2023) 100487

Contents lists available at ScienceDirect

Results in Optics

journal homepage: www.sciencedirect.com/journal/results-in-optics

Dose responses of scattered- and direct-X-ray-irradiated CR-39 and methylviologen-encapsulated silica nanocapsule-doped CR-39 and their mechanisms

Hirokazu Miyoshi [a,*], Fumio Kida [b], Kenji Yamada [c], Mami Nakamura [a], Hitoshi Hase [b]

[a] Advance Radiation Research, Education, and Management Center, Tokushima University, 3-18-15 Kuramoto-cho, Tokushima 770-8503, Japan
[b] SUN•LUX Optical Co., Ltd., 3-5-25 Maruyama-cho, Sabae City, Fukui 916-0019, Japan
[c] Tokushima University Hospital, 2-50-1 Kuramoto-cho, Tokushima 770-8503, Japan

ARTICLE INFO

Keywords:
Direct X-ray
Scattered X-ray
CR-39
Photoexcited emission
Dose response
Silica nanocapsule

ABSTRACT

The photoexcited emissions of direct- and scattered-X-ray-irradiated CR-39 and methylviologen-encapsulated silica nanocapsule (MV^{2+}@SiO_2 NC)-doped CR-39 were observed, and they showed a dose response. The benzophenone radical was formed in a shallow trap in CR-39 upon X-ray irradiation from 10 to 30 Gy, and the fluorescence intensity increased with the dose. Methylviologen in SiO_2 NCs competitively captured electrons generated by X-ray irradiation, and the captured electrons were reverse transferred to the shallow traps with time. A minimum dose rate of 300 μGy/s was observed between 1 and 5 Gy. Finally, a dose response of less than 2 mGy for scattered X-rays was obtained in this system.

1. Introduction

CR-39 made of polyallyl diglycol carbonate (PADC), which is transparent and colorless, was polymerized using diisopropyl peroxydicarbonate (IPP) as a polymerization initiator (Ahmad and Stejny, 1991). The CR-39 was used as a glass lens containing a UV absorber such as 2-hydroxy-4-methoxybenzophenone (HOMtOBP). Recently, the thermally activated delayed fluorescence of HOMtOBP in host–guest complexation has been studied (Koninti et al., 2021). CR-39 was also studied and used as a well-known solid-state dosimeter to detect alpha particles (Frutos-Puerto et al., 2021) and neutron flux (Kading et al., 2020). After it was exposed to both types of radiation, alkali etching was performed, and the formed pore size and its depth were observed under an optical microscope to evaluate the dose (Sabbarese et al., 2020). Up to now, many studies on CR-39 have been reported. Nowadays, it is used to detect biomaterials with a surface-enhanced Raman material in biomaterial sensing (Taha et al., 2021). However, the same CR-39 cannot be reused in dosimetry because of alkali etching.

In all tasks of physicians performing X-ray fluoroscopy and interventional radiology (IVR) in hospitals, exposure dose is very important (Inaba et al., 2021; Endo et al., 2021). Usually, a personal dosimeter such as a glass badge is attached to the body under a Pb protector and behind Pb glass. The exposure dose of the glass badge is not measured in situ, but after one month of use. Therefore, in situ visualization of the exposure dose of X-rays is useful and necessary. On the other hand, GAFchromic film (International Specialty Products) has been a well-known dosimetry tool for patient use since 2011. Also, GAFchromic external beam therapy (EBT)-high-dose extended model (XD) film has been developed to measure absorbed doses in the range between 0.4 and 40 Gy (Santos et al., 2021). Recently, Tamura et al. have reported on a photochromic diarylethene film acting as a clinical dosimeter for 150 kV X-rays using fluorescence spectra and its images (Tamura et al., 2021). However, until now, there have been no studies on the visualization of X-rays and its dose with in situ measurement for physicians exposed to X-rays.

A new property of CR-39 of detecting X- and gamma rays without alkali etching and the effect of doping with methylviologen-encapsulated silica nanocapsules (MV^{2+}@SiO_2 NCs) have been reported (Miyoshi et al., 2015). It has taken almost eight years to measure the dose response of CR-39 using emission generated by irradiating excitation light (Miyoshi et al., 2016), and the visualization of X-rays with CR-39 was performed using the fluorescence generated upon laser or LED excitation (Miyoshi et al., 2019). To enable the practical use of this dosimetry, the dose response and dose rate dependence must be known.

In this paper, some evaluations of the obtained results of dose and

* Corresponding author.
E-mail address: miyoshi.hirokazu@tokushima-u.ac.jp (H. Miyoshi).

https://doi.org/10.1016/j.rio.2023.100487
Received 12 February 2023; Received in revised form 27 June 2023; Accepted 5 July 2023
Available online 10 July 2023

dose rate responses are conducted, and their mechanisms in CR-39 and $MV^{2+}@SiO_2$ NC-doped CR-39 ($MV^{2+}@SiO_2$ –CR-39) are proposed. The following points are discussed.

1) The role of $MV^{2+}@SiO_2$ NCs in X-ray-irradiated $MV^{2+}@SiO_2$ NC-doped CR-39 is to enhance the fluorescence intensity in a 1-mm-thick plate for 30 kV X-rays and to decrease the fluorescent image intensity in a 9-mm-thick rod for 80 kV X-rays. Those causes were discussed.
2) The intensity or area of a fluorescence spectrum was proportional to a dose of more than 0.5 Gy of X-rays (80 kV). The dose rate dependence was investigated at 1 and 5 Gy.
3) The dose response between 0 and 2 mGy of scattered X-rays (80 kV) is clarified using the emission image intensity distribution. Pre–X-ray (80 kV)-irradiated CR-39 (30 Gy) had enhanced sensitivity for a dose of less than 2 mGy of scattered X-rays.

2. Materials and methods

2.1. Reagents

$KAuCl_4$, sodium silicate solution, $NaSi_xO_{2-x}$ (28 wt% SiO_2), 3-aminopropylorthosilicate (APS), and sodium citrate were purchased from Sigma-Aldrich Co., Ltd. Concentrated NH_4OH, MV^{2+}, and ethyl alcohol were purchased from Wako Co., Ltd. The UV absorber, 2-hydroxy-4-methoxybenzophenone (HARI sorb 101), was purchased from Harima Kasei Co., Ltd. The polymerization initiator used was IPP. Ultrapure water was obtained with a Barnstead EasyPure RoDi water purification system (Thermoscientific Co., Ltd.). These reagents were used without further purification.

2.2. Preparation of $MV^{2+}@SiO_2$ NC-doped CR-39

An aqueous dispersion of $MV^{2+}@SiO_2$ NCs was prepared by the core–shell method (Miyoshi et al., 2016). As the core, Au nanoparticles (NPs) of 15 nm diameter were prepared by citrate reduction. After MV^{2+} was added to a Au NP aqueous dispersion, APS was added and the mixture was stirred at room temperature. Then silicate solution was added to the dispersion to form silica shells. After one week of stirring, the dispersion was ultrafiltrated with a 100 kDa membrane filter and washed with pure water several times. Figure S1 (a) shows an absorption spectrum of $MV^{2+}@SiO_2$ NC aqueous dispersion. As shown in Fig. S1(a), a typical absorption peak at 260 nm of MV^{2+} was observed even after washing with pure water several times, indicating MV^{2+} incorporation into SiO_2 NCs or in a layer of SiO_2. Figure S1(b) shows a TEM image of $MV^{2+}@SiO_2$ NCs and each red arrow shows an empty capsule. The obtained $MV^{2+}@SiO_2$ NC aqueous dispersion was replaced with ethyl alcohol by ultrafiltration and its ethyl alcohol dispersion was obtained.

In the preparation of $MV^{2+}@SiO_2$ –CR-39, a line polymerization furnace for CR-39 was used. After polyallyl diglycol carbonate containing 5.6% IPP and a 4000 ppm UV absorber and four types of $MV^{2+}@SiO_2$ ethyl alcoholic dispersion (ratio of $MV^{2+}@SiO_2$ to $MV^{2+}@SiO_2$–CR-39: 0.5, 1, 2, and 3) were mixed completely, they were polymerized in a line polymerization furnace. $MV^{2+}@SiO_2$ –CR-39 (ratio of $MV^{2+}@SiO_2$ to $MV^{2+}@SiO_2$–CR-39: 0.5, 1, 2, and 3) rods of 0.7 cm × 5 cm × 0.9 cm (W × D × H) and $MV^{2+}@SiO_2$ –CR-39 (ratio of $MV^{2+}@SiO_2$ to $MV^{2+}@SiO_2$–CR-39: 0.5, 1, 2, and 3) plates of 1 cm × 5 cm × 0.1 cm (W × D × H) were obtained.

TEM images of the cross section of the 9-mm-thick $MV^{2+}@SiO_2$ –CR-39 rod were observed to elucidate the distribution of $MV^{2+}@SiO_2$ NCs (Figs. S2(a-1)–(e-1)) using a JEOL transmission electron microscope (JEOL Co. Ltd., JEM-2100F). The cross section was prepared by the ultrathin section method using a microtome (LKB Co., Ltd., 2088ULTROME V) with a diamond knife (SYMTEC Co., Ltd. SYM Knife 0545). Some sample decay images obtained by the ultrathin section method were observed. With an increase in the ratio of $MV^{2+}@SiO_2$, the number of some dark points increased (Figs. S2 (b-1)–(d-1)) and a large dark area corresponding to aggregation appeared (Fig. S2(e-1)). SEM-EDS and element analysis (Figs. S2(a-2)–(e-2)) of these cross sections were performed using a scanning electron microscope (JEOL JSM-6510HV). However, there are no peaks of Si K in these samples, because the sensitivity was insufficient for the detection of $MV^{2+}@SiO_2$ in CR-39 by SEM-EDS.

2.3. X-ray irradiation experiments

2.3.1. Direct X-ray irradiation

X-rays of 30 kV were obtained with a Rigaku Rint II X-ray diffractometer without calibration. X-rays of 80 kV were irradiated from MX-80Labo (MediXtec Co., Ltd.), where an EMF 521B dosimeter with a 0.3 cm fingertip chamber (PTW-Freiburg, Semiflex Chamber Type 31013) was used to calibrate the dose. Then, a dose rate of 3.38 Gy/min at a distance of 10 mm between the irradiation window and the sample was obtained by adjusting the irradiation time using MX-80Labo control software. X-rays of 80 kV were also irradiated onto the samples, which were covered with 20 pieces of 10-mm-thick acryl plates (20 mm × 20 mm) to maintain the output power of X-rays, on a table from the bottom direction using the Allura Xper FD20/20 biplane neuro X-ray system (Philips Electronics Co., Ltd.) at Tokushima University Hospital. The dose at a table surface 120 cm from the floor was calibrated by confirming the value indicated in the dosimeter at 4 frame/s of the Allura Clarity ver.81305 FD20/20 biplane. Each sample was removed after X-ray irradiation at each dose.

Figure S3 shows the relationship between the thickness and I/I_0 with 30 and 80 kV X-rays for CR-39 plates. As shown in Fig. S3, the 80 kV X-rays at Tokushima University Hospital almost completely penetrated the 0.1-cm-thick CR-39 plates.

2.3.2. Scattered X-ray irradiation

X-rays of 80 kV from the bottom direction were irradiated onto 20 pieces of 10-mm-thick acryl plates (20 mm × 20 mm) on a 120-cm-high table and were scattered in the perpendicular direction, where CR-39

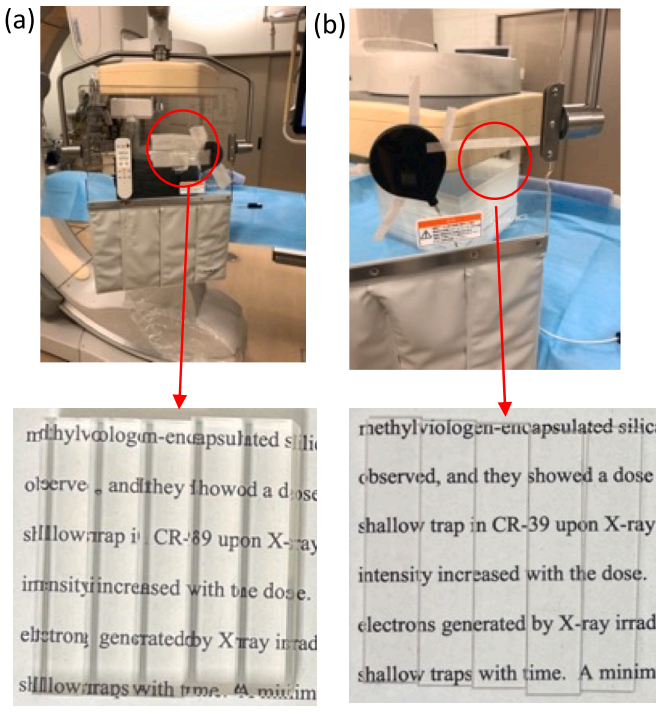

Fig. 1. Photographs of (a) CR-39 rods and (b) plates for scattered X-ray irradiation. Arrows indicate close-ups of CR-39 rods and plates.

rods or plates were attached to the acryl Pb shield plate at a height of 150 cm from the floor, as shown in Fig. 1.

The irradiation was performed every 10 s 13 times, and the total exposure dose was 2.078 mGy on the surface of an acryl Pb shield plate. The dose was calibrated using an 10X6-60 ion chamber (Radcal Co., Ltd.) by confirming the value indicated in the dosimeter at 4 frame/s of the Allura Clarity ver.81305 FD20/20 biplane.

Two sets of 0.7 cm × 5 cm × 0.9 cm MV^{2+}@SiO_2 –CR39 (0.5, 1, 2, 3) rods and three sets of 0.7 cm × 5 cm × 0.9 cm CR-39 rods were placed on the surface of the acrylic Pb shield plate near the dosimeter, as shown in Fig. 1(a),(b). Each sample was removed after each dose of X-ray irradiation.

2.4. Attenuation coefficient for CR-39 and MV^{2+}@SiO_2

The total attenuation coefficient with coherent scattering against photon energy from 0.001 to 2 MeV was calculated using the NIST XCOM online resource (NIST-XCOM, 2023). The formulas for compound were C12H18O7 for CR-39 and C12H14Cl2N2SiO2 for MV^{2+}@SiO_2. Figure S4 shows the total attenuation coefficient with coherent scattering against photon energy for CR-39 and MV^{2+}@SiO_2. The total attenuations at 30 and 80 kV for CR-39 and MV^{2+}@SiO_2 were 0.313 and 0.867 m^2/g and 0.174 and 0.198 m^2/g, respectively.

2.5. Optical measurements

Fluorescence spectra were measured using Shimadzu RF5300PC with a quartz cell. Fluorescent images were observed with the FLA-9000 imager (Fuji Film Co., Ltd.) and their intensities per area were measured with ImageJ software. The obtained intensities were averaged and plotted against the dose or ratio of MV^{2+}@ SiO_2 NCs to MV^{2+}@ SiO_2–CR-39 using Igor Pro 9 software (WaveMetrics) or Excel software (Microsoft).

3. Results and discussion

3.1. Fluorescence mechanism of X-ray-irradiated CR-39

The fluorescence mechanism of X-ray-irradiated CR-39 has been reported as follows (Miyoshi et al., 2015).

$$\text{X - ray} \rightarrow \text{CR - 39}(e^- + h^+) \quad (1)$$

$$e^- + \text{trap level (shallow or deep)} \rightarrow (e^-) \text{ in trap level (shallow or deep)} \quad (2)$$

$$(e^-) \text{ in trap level (shallow or deep)} + hv \rightarrow \text{fluorescence} \quad (3)$$

The shallow trap may be due to the UV absorber and polymerization initiator in CR-39 because when their contents increased, the fluorescence intensity increased, as previously reported (Miyoshi et al., 2016). Moreover, after X-ray (30 kV, 15 mA) irradiation of 1-mm-thick CR-39, the intensity of the radio-photoluminescent image, which was excited at 555 nm, was kept constant by adjusting the concentration of MV^{2+} @ SiO_2 NCs doped into CR-39 (Miyoshi et al., 2015). One role of MV^{2+} @ SiO_2 NCs in X-ray-irradiated CR-39 is to enhance the fluorescence intensity at the 1-mm-thick plate for 30 kV X-rays. The deep trap may be due to MV^{2+} @ SiO_2 NCs in MV^{2+}@SiO_2 NC-doped CR-39, as shown later.

3.2. Fluorescence spectra of X-ray-irradiated CR-39 and dose dependence of fluorescence intensity

Fig. 2(a) shows the fluorescence spectra of an X-ray (80 kV)-irradiated 9-mm-thick CR-39 rod against dose. As shown in Fig. 2(a), a peak at 580 nm upon excitation at a wavelength of 535 nm was observed depending on the dose, and its intensity increased with dose. This is the origin of the fluorescent image observed with the FLA-9000 imager. In

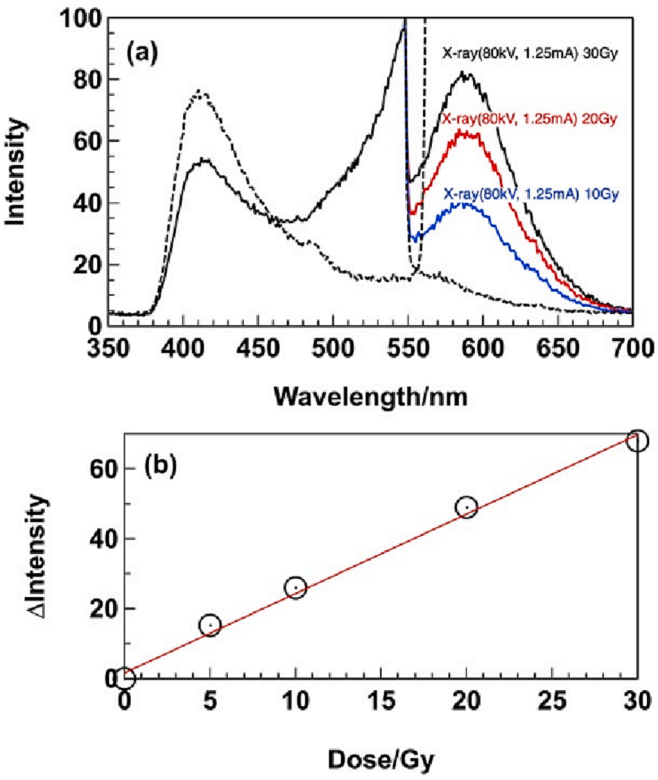

Fig. 2. (a) Excitation and emission spectra of 9-mm-thick CR-39 rod upon irradiation of X-rays (80 kV, 1.25 mA). Dose: 10 Gy, 20 Gy, 30 Gy. (b) Dose dependence of ΔIntensity of X-ray-irradiated 9-mm-thick CR-39 rod.

contrast, the fluorescence intensity at 470 nm upon excitation at a wavelength of 405 nm did not change, even with different doses. A plot of net intensity minus the background intensity against dose indicated a linear relationship (Slope = (2.27 ± 0.111) and $r^2 = 0.995249$ obtained using IgorPro software), as shown in Fig. 2(b). Electrons were trapped in the trap sites of CR-39 upon X-ray irradiation and the fluorescence peak intensity linearly increased with dose, indicating that this CR-39 can be employed as a dosimeter in the range of 0 to 30 Gy by using the fluorescence peak intensity.

The above results indicated that fluorescent centers were generated in CR-39 upon X-ray irradiation. The fluorescence spectra were in agreement with those of benzophenone and their radicals (Sakamoto et al., 2006) added to CR-39 as UV absorbers. Haogang et al. reported that irradiation of 5 Gy of 2–4 MeV electron pulses generated ketyl radicals of benzophenone (Jin et al., 1996). Since the X-ray energies are 30 and 80 kV and the redox potential of MV^{2+} is − 0.69 V vs SCE (Ward et al., 1983) and that of benzophenone is − 1.9 V vs SCE (NIST-XCOM, 0000), it is easy to reduce them in CR-39.

Otherwise, as the oxidation potential of the benzophenone radical is − 0.25 V vs SCE (Sakamoto et al., 2006), the benzophenone radical is unstable. In the presence of MV^{2+} @ SiO_2 NCs, the generated electron was captured by MV^{2+}, leading to a decrease in the fluorescence intensity. This clarifies that the fluorescence intensity or Δarea is proportional to the dose from 0.5 to 2.5 Gy, as shown in Fig. 3. Each slope is approximated to be (467.22 ± 22.5) with $r^2 = 0.99531$ for 9-mm-thick CR-39 and (342.71 ± 30.4) with $r^2 = 0.977009$ obtained using Igor Pro software for the MV^{2+}@SiO_2 –9-mm-thick CR-39 rod with a ratio of 3 of MV^{2+} @SiO_2 NCs. In the presence of MV^{2+} @ SiO_2 NCs, the slope of Δarea against dose decreased because the redox potential of MV^{2+} is lower than that of benzophenone. Furthermore, since MV^{2+} @SiO_2 is wholly distributed in CR-39 and its total attenuation coefficient is larger than that of 2-hydroxy-4-methoxybenzophenone (0.173 m^2/g for 30 kV and 0.2871 m^2/g for 80 kV of photon energy calculated using NIST

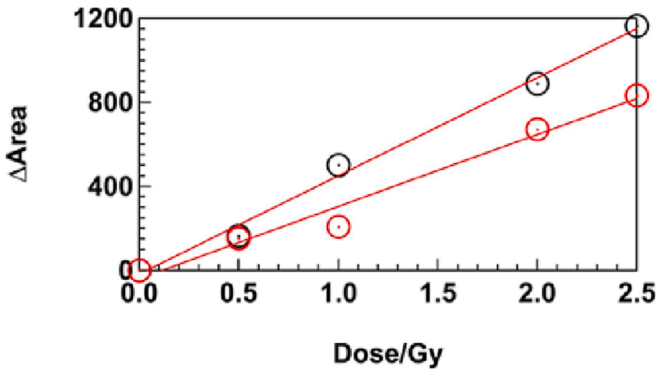

Fig. 3. Dose dependence of X-ray-irradiated 9-mm-thick CR-39 rod (black circles) and MV^{2+}@SiO_2 –9-mm-thick CR-39 rod with a ratio of 3 of MV^{2+} @SiO_2 NCs in MV^{2+}@ SiO_2–CR-39 (red circles). (For interpretation of the references to color in this figure legend, the reader is referred to the web version of this article.)

XCOM), in the presence of MV^{2+} @ SiO_2 NCs, the photon energy may be preferentially captured by MV^{2+} @ SiO_2 NCs. Therefore, Δarea against dose decreased for the MV^{2+}@SiO_2 –9-mm-thick CR-39 rod. The absorption spectra in Fig. S5 (a)(b) indicate the formation of $MV^{+\bullet}$ in MV^{2+} aqueous solution and MV^{2+} @ SiO_2 NC aqueous dispersion upon 80 kV X-ray irradiation with 321 Gy. As shown in Fig. S5(c), in the case of MV^{2+} @ SiO_2NCs, their absorbances at 395 nm, which was due to $MV^{+\bullet}$ (Wolszczak, 1989), was almost saturated ($[Absorbance] = (0.015329 \pm 0.0671) + (0.0063154 \pm 0.00101) \times [dose] - (8.4845e-06 \pm 3.03e-06) \times [dose]^2$, V_chisq = 0.00473946), and the blue color of the solution based on $MV^{+\bullet}$ remained being allowed to stand or one day (Fig. S5 (d)), indicating that MV^{2+} in SiO_2 NCs and X-ray-excited electrons could reduce MV^{2+} to $MV^{+\bullet}$ in SiO_2 NCs.

The linearity between Δarea and dose within 0 to 2.5 Gy indicated that this CR-39 and MV^{2+}@SiO_2 –CR-39 can be used as dosimeters in the range from 0 to 2.5 Gy, using the area of the fluorescence spectrum. It will be easy to visualize the absorbed X-ray doses of 0 to 2.5 Gy and 0 to 30 Gy using this CR-39 and MV^{2+}@SiO_2 –CR-39.

3.3. Dose rate dependence

Fig. 4 shows the dose rate dependence for 1 and 5 Gy of X-rays (80 kV).

In the case of a low dose rate, the intensity and area decreased to 87% for 5 Gy of X-rays (80 kV, 0.12 mA), as shown in Fig. 4. In the case of 1 Gy, the dose rate decreased markedly to 20% (80 kV, 0.12 mA), indicating that the dose rate depends on the X-ray dose, as shown in Fig. 4.

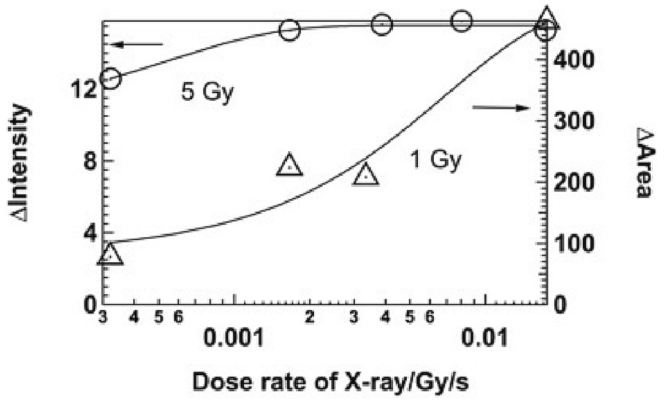

Fig. 4. Plot of ΔIntensity (dose: 5 Gy) and ΔArea (dose: 1 Gy) vs dose rate of X-rays (80 kV) for 9-mm-thick CR39 rod.

The decrease in the dose from 5 to 1 Gy indicated that the response of CR-39 decreased at the same dose rate. The minimum dose rate indicated the minimum area, that is, the dose rate limit for producing the desired benzophenone radical in CR-39, and is about 300 μGy/s for X-rays (80 kV, 0.12 mA), as determined using the peak intensity or area.

Fig. 5 shows the response to doses less than 20 mGy, determined using the fluorescent image intensities for X-ray-irradiated CR-39 and MV^{2+}@SiO_2 –CR-39. A fluorescent image with a 100 μm resolution was obtained from the fluorescence of the X-ray-irradiated 9-mm-thick CR-39 rod and MV^{2+}@SiO_2 –CR-39 excited by a 532 nm laser using an FLA-9000 fluoroanalyzer.

The obtained fluorescent image was analyzed from the plot profile using in ImageJ software. More data are obtained for the intensity from the fluorescent image than for the intensity and area in the fluorescence spectrum because the fluorescence intensity is generated from the whole body. Therefore, even at a dose less than 20 mGy, the intensity is detectable. The detection of a dose less than 20 mGy is reasonable for the detection of 300 μGy/s of X-rays, as shown in Fig. 5(a). When the relative concentration of MV^{2+} @ SiO_2 NCs increased, the normalized slope of image intensity decreased, as shown in Fig. 5(b).

3.4. Detection of exposure dose of scattered X-rays using fluorescent images of CR-39 and MV^{2+}@SiO_2 –CR-39

Several types of MV^{2+}@SiO_2–CR-39 rod were prepared; the four faces were transparent and clear. Before X-ray exposure, their fluorescent images were measured at 532 nm excitation using FLA-9000. After that, scattered X-rays were irradiated every 10 s for a total absorbed dose of 2.078 mGy. The dose rate was about 208 μGy/s, which is lower than the 300 μGy/s obtained in the previous experiment. The fluorescent

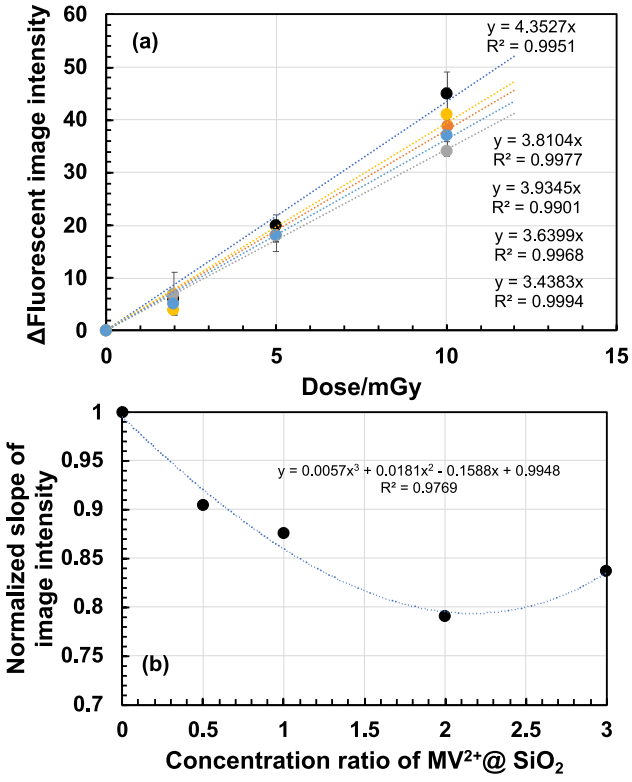

Fig. 5. (a) Plot of ΔFluorescent image intensity for several concentration ratios of MV^{2+}@SiO_2 NCs (0 (black circles), 0.5 (orange circles), 1 (gray circles), 2 (yellow circles), 3 (blue circles)) in 9-mm-thick CR39 rod vs dose. (b) Plot of normalized slope of fluorescent image intensity from Fig. 5(a) vs concentration ratio of MV^{2+}@SiO_2 NCs in CR-39. (For interpretation of the references to color in this figure legend, the reader is referred to the web version of this article.)

images excited at 532 nm of all scattered-X-ray-irradiated 9-mm-thick $MV^{2+}@SiO_2$ –CR-39 rods for two sets were measured using the FLA-9000 imager. Their intensities were measured using the plot profile of ImageJ; the intensity profiles are shown in Fig. 6(a) and (b).

The difference in intensity between before and after scattered X-ray irradiation is indicated in the figure. All 9-mm-thick $MV^{2+}@SiO_2$ –CR-39 rods indicated an increased intensity after X-ray exposure. The X-ray dose of 2.078 mGy can be detected clearly when square $MV^{2+}@SiO_2$ –CR-39 rods are used. The fluorescence intensity of all fluorescent images increased within 1 day after 647 nm laser irradiation, even that of CR-39 only, and at almost the same rates, indicating that most of the X-ray irradiation energy may be accumulated in CR-39 at such a low dose, causing reverse electron transfer to the benzophenone radical with time. After three days, the intensities of the fluorescent image decreased to less than the initial intensity, indicating that the CR-39 and $MV^{2+}@SiO_2$ –CR-39 rods can be reused for X-ray detection.

On the other hand, 1-mm-thick $MV^{2+}@SiO_2$ –CR-39 plates did not show such increased fluorescence intensities, rather, the intensities of the fluorescent image decreased after one day, as shown in Fig. S6(a). However, the rate of decrease in the fluorescence intensity of 1-mm-thick CR-39 plates was higher than that of 1-mm-thick $MV^{2+}@SiO_2$ –CR-39 plates (Fig. S6(b)), indicating that electrons captured by $MV^{2+}@SiO_2$ transferred to biphenyl radicals with time or 647 nm laser irradiation. Thus, in the case of the 1-mm-thick plates, the effect of $MV^{2+}@SiO_2$ on keeping electrons for one day was observed. The causes are attributed to the uniformity of $MV^{2+}@SiO_2$ NCs in CR-39. The $MV^{2+}@SiO_2$ NC dispersions were not uniformly distributed in the 9-mm-thick CR-39 rods, but were distributed uniformly in the 1-mm-thick CR-39 rods, as shown by the fluorescence spectra of $MV^{2+}@SiO_2$ in CR-39 (data not shown). On the other hand, the HOMtOBP molecules were uniformly mixed in CR-39 as UV absorbers. Therefore, the effect of using the 1-mm-thick $MV^{2+}@SiO_2$ –CR-39 plates was that $MV^{2+}@SiO_2$ kept electrons for one day.

3.5. Enhanced sensitivity of pre–X-ray-irradiated CR-39 to scattered X-ray doses less than 2 mGy

The response to doses less than 2 mGy of scattered X-rays was investigated using the fluorescent image intensity ratio, that is, the ratio of pre–X-ray-irradiated fluorescent image intensity to that before irradiation, for each dose less than 2 mGy. Furthermore, pre-X-ray irradiation was performed at 0, 15, and 30 Gy on each of the five CR-39 rods. For example, Fig. 7(a) shows the difference in fluorescence image intensity between without (blue solid circle) and with (orange solid circle) 30 Gy of pre–X-ray irradiation for CR-39 against the dose of scattered X-ray irradiation. The ratios of the slope were 0.67 for without pre–X-ray irradiation, 1.04 for 15 Gy of pre–X-ray irradiation, and 1.3 for 30 Gy of pre–irradiation, as shown in Fig. 7(b). Pre–X-ray irradiation led to the production of more benzophenone radicals in CR-39, and the total fluorescence intensity increased. This indicates that under the

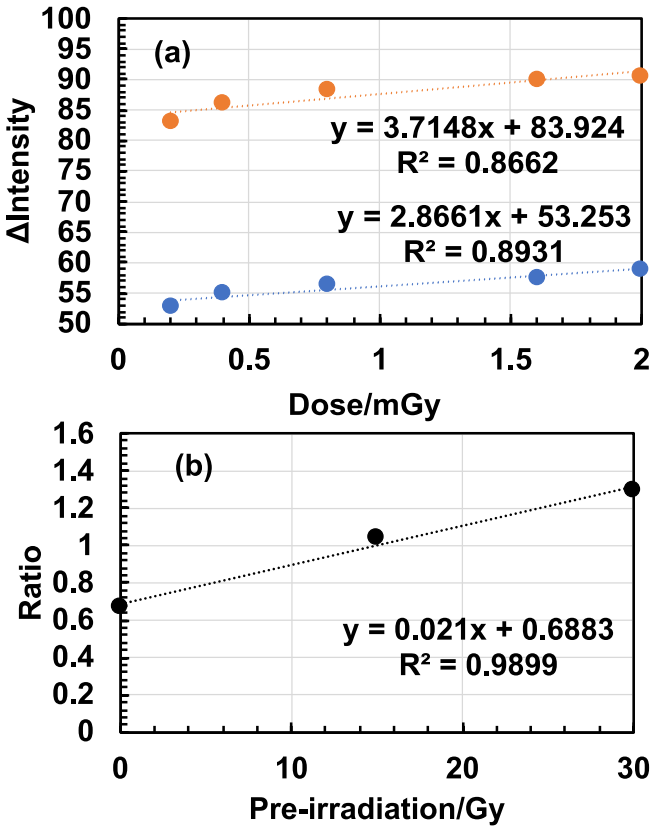

Fig. 7. (a) Plot of Δintensity without (blue circles) and with (orange circles) 30 Gy of pre–X-ray irradiation vs dose. (b) Plot of ratio of the slope (Fig. 7 (a) for 30 of Gy pre–X-ray irradiation) vs pre–X-ray-irradiation dose for 9-mm-thick CR39 rod. (For interpretation of the references to color in this figure legend, the reader is referred to the web version of this article.)

circumstance of more benzophenone radicals in CR-39, the benzophenone radicals were easily formed even by low-dose X-ray irradiation. As shown in Fig. 7(b), the ratio of over 1 was due to pre–X-ray irradiation at 15 and 30 Gy. Therefore, the five 30 Gy pre–X-ray-irradiated CR-39 rods were covered with 4-mm-thick Pb plates at each scattered X-ray dose and their fluorescent images were obtained. For example, plot profiles before and after X-ray irradiation and the fluorescent image intensity ratio for one rod are shown in Fig. 8(a), (b), and (c). Fig. 8(c) shows a plot of the ratio against distance. The distance is the distance covered by the Pb plate on each step, which corresponds to the dose. Fig. 8(d) shows the average ratio vs dose.

As shown in Fig. 8(d), the scattered X-ray dose could be measured up to less than 2 mGy with the slope of 0.0058. The four other CR-39 rods

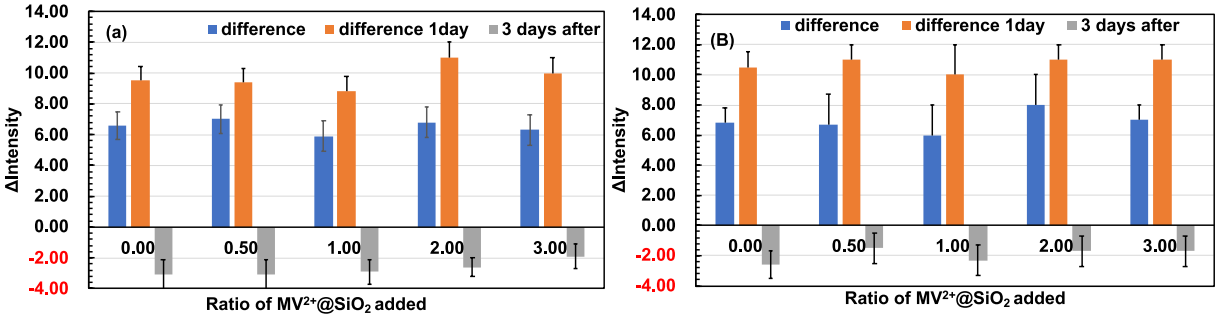

Fig. 6. (a)(b) Plots of Δintensity for immediately after scattered X-ray irradiation (blue bars: difference), after 1 day (orange bars: difference 1 day), and after 3 days (gray bars: 3 days after) against ratio of MV^{2+} @ SiO_2 added or two sets of 9-mm-thick $MV^{2+}@SiO_2$-CR-39 rods. Total dose of scattered X-ray: 2.078 mGy (10 repetitions of irradiation each for 10 s). (For interpretation of the references to color in this figure legend, the reader is referred to the web version of this article.)

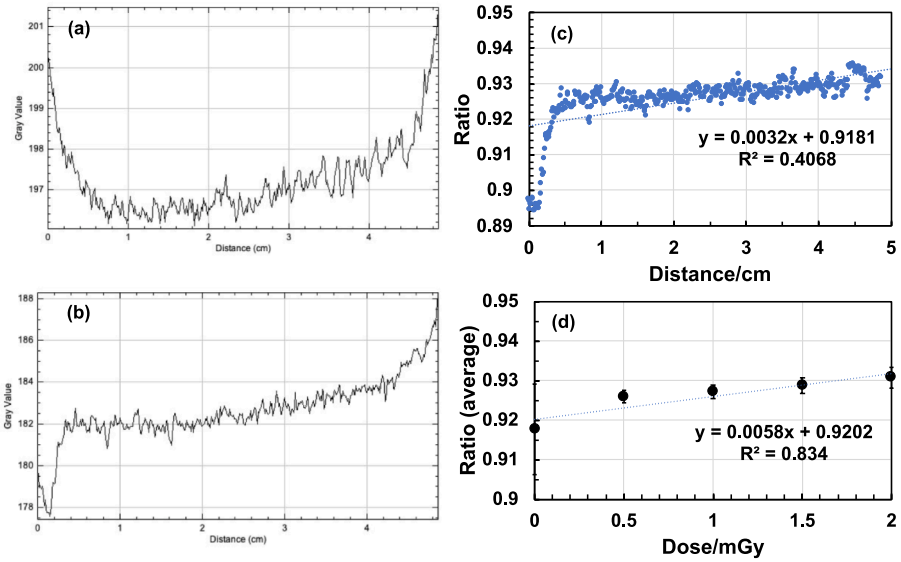

Fig. 8. Plot of gray values for fluorescent image of CR-39 covered by Pb plate step by step before (a) and after (b) X-ray irradiation. (c) Plot of ratio of gray values after (b) against before (a) X-ray irradiation vs distance covered by Pb plate step by step. (d) Plot of average ratio (c) for each distance irradiated by X-rays against dose.

indicated that the slopes between the average ratio and the dose were 0.0049, 0.0057, 0.0051, and 0.0027. The average and standard deviation were 0.005 and 0.001, respectively. Finally, pre–X-ray irradiation may cause sensitivity to small X-ray doses of less than 2 mGy because of the generation of benzophenone radical residues.

4. Conclusion

CR-39 and MV^{2+}@SiO_2 –CR-39 exhibited some photoemission properties applicable to X-ray detection. Benzophenone radicals were formed in CR-39 upon X-ray irradiation at 10 to 30 Gy, and the fluorescence intensity increased with the dose. Methylviologen in SiO_2 NCs competitively captured electrons generated by X-ray irradiation, which were reverse transferred to shallow traps. A dose rate of 300 μGy/s was observed for scattered X-rays of 1 and 5 Gy. Finally, CR-39 rods could be used to detect a dose less than 2 mGy of scattered X-rays using fluorescent images.

Funding

This work was supported by SUN•LUX Optical Co., Ltd., Sabae, Japan.

Declaration of Competing Interest

The authors declare that they have no known competing financial interests or personal relationships that could have appeared to influence the work reported in this paper.

Data availability

The authors are unable or have chosen not to specify which data has been used.

Acknowledgements

We profoundly thank Mr. Tomoyuki Ueki of the Institute of Technology and Science Center of Tokushima University for technical support in the TEM observations of CR-39 with and without MV^{2+}@SiO_2 NCs. We sincerely thank SUN•LUX Optical Co., Ltd., Sabae, Japan, for their support.

Appendix A. Supplementary data

Supplementary data to this article can be found online at https://doi.org/10.1016/j.rio.2023.100487.

References

Ahmad, S., Stejny, J., 1991. Polymerization, structure and track recording properties of CR-39. Nucl. Tracks Radiat. Meas. 19 (1–4), 11–16. https://doi.org/10.1016/1359-0189(91)90135-5.

Endo, M., Haga, Y., Sota, M., Tanaka, A., Otomo, K., Murabayashi, Y., Abe, M., Kaga, Y., Inaba, Y., Suzuki, M., Meguro, T., Chida, K., 2021. Evaluation of novel X-ray protective eyewear in reducing the eye dose to interventional radiology physicians. J. Radiat. Res. 62 (3), 414–419. https://doi.org/10.1093/jrr/rrab014.

Frutos-Puerto, S., Hurtado-Sanchez, M.C., Pérez, J.T., Pinilla-Gil, E., Miró, C., 2021. Radon alpha track counting on solid state nuclear track detector by an ImageJ-based software macro. Appl. Radial. Isot. 173, 109695 https://doi.org/10.1016/j.apradiso.2021.109695.

Inaba, Y., Hitachi, S., Watanuki, M., Chida, K., 2021. Occupational radiation dose to eye lenses in CT-guided interventions using MDCT-fluoroscopy. Diagnostics 11 (4), 1–9. https://doi.org/10.3390/diagnostics11040646.

Jin, H., Pan, X., Wu, J., Li, F., Lui, A., L., and Gu, H., Microsecond pulse radiolysis of benzophenone tributyl phosphate system, *Radiat. Phys. Chem.,* **47**(6), 815–816, 1996. https://doi.org/10.1016/0969-806X(95)00154-P.

Kading, E.E., Aviv, O., Eliyahu, I., Gai, M., Halfon, S., Hass, M., Howell, C.R., Kijel, D., Mishnayot, Y., Mukul, I., Perry, A., Shachar, Y., Seiffert, C., Shor, A., Silverman, I., Stern, S.R., Stora, T., Ticehurst, D.R., Weiss, A., Weissman, L., 2020. Tests and calibrations of nuclear track detectors (CR39) for operation in high neutron flux. Phys. Rev. Res. 2 (2), 23279. https://doi.org/10.1103/PhysRevResearch.2.023279.

Koninti, R.K., Miyata, K., Saigo, M., Onda, K., 2021. Achieving thermally activated delayed fluorescence from benzophenone by host-guest complexation. J. Phys. Chem. C 125, 17392–17399. https://doi.org/10.1021/acs.jpcc.1c04283.

Miyoshi, H., Kida, F., Hase, H., Tsuchiya, K., 2015. Silica-nanocapsule-doped CR-39 for fluorescence detection of X-rays. Phys. Procedia 80, 90–93. https://doi.org/10.1016/j.phpro.2015.11.100.

Miyoshi, H., Kida, F., Yamada, K., Tsuchiya, K., Hase, H., 2016. Optical property of CR-39 synthesized by doping with methylviologen-encapsulated SiO_2 nanocapsules as a solid-state X-ray plate detector. Opt. Mater. 55, 109–114. https://doi.org/10.1016/j.optmat.2016.02.042.

Miyoshi, H., Kida, F., Kawase, Y., Yamada, K., Sasaki, M., Shoji, H., Hase, H., 2019. Emission image of X-ray-irradiated CR-39 stick doped with methylviologen-encapsulated silica nanocapsules using LED light. Prog. Nucl. Sci. Technol. 6, 91–94. https://doi.org/10.15669/pnst.6.91.

NIST XCOM online resource: https://physics.nist.gov/PhysRefData/Xcom/html/xcom1.html.

Sabbarese, C., Ambrosino, F., Roca, V., 2020. Analysis by scanner of tracks produced by radon alpha particles in CR-39 detectors. Radiat. Protec. Dosim. 91 (2), 154–159. https://doi.org/10.1093/rpd/ncaa140.

Sakamoto, M., Cai, X., Fujisuka, M., Majima, T., 2006. Solvent effect on the deactivation processes of benzophenone ketyl radicals in the excited state. J. Phys. Chem. A 110, 11808–11900. https://doi.org/10.1021/jp060129g.

Santos, T., Ventura, T., Lopes, M.C., 2021. A review on radiochromic film dosimetry for dose verification in high energy photon beams. Radiat. Phys. Chem. 179, 109217 https://doi.org/10.1016/j.radphyschem.2020.109217.

Taha, R., Jawad, H., Parvin, P., Mitra, R., 2021. Modification of CR39 surfaces by 193 nm ArF laser for biomaterial sensing. *Mater. Today*: *Proc.* 42, 2273–2276. https://doi.org/10.1016/j.matpr.2020.12.315.

Tamura, M., Monzen, H., Matsumoto, K., Otsuka, M., Nishimura, Y., 2021. Feasibility study of a photochromic diarylethene film as a clinical dosimeter for kV X-rays. Radiat. Meas. 146, 106608 https://doi.org/10.1016/j.radmeas.2021.106608.

Ward, M.D., White, J.R., Bard, A.J., 1983. Electrochemical investigation of the energetics of particulate titanium dioxide photocatalysts. The methylviologen-acetate system. J. Am. Chem. Soc. 105, 27–31. https://doi.org/10.1021/ja00339a007.

M. Wolszczak and Cz. Stradowski, Methylviologen cation radical, its dimer and complex in various media, *Radiat. Phys. Chem.*, **33**(4), 355–359, 1989. https://doi.org/10.1016/1359-0197(89)90033-7.